

Understanding Periodic Dislocations in 2D Supramolecular Crystals: The PFP/Ag(111) Interface

E. Goiri,[†] J. M. García-Lastra,[‡] M. Corso,[†] Z. M. Adb El-Fattah,[¶] J. E. Ortega,^{†,¶,||} and D. G. de Oteyza*,^{¶,§}

[†]Donostia International Physics Center, Paseo Manuel Lardizabal 4, E-20018 Donostia-San Sebastián, Spain

[‡]Department of Physics, Technical University of Denmark, DK-2800 Copenhagen, Denmark

[¶]Centro de Física de Materiales CSIC/UPV-EHU-Materials Physics Center, E-20018 Donostia-San Sebastián, Spain

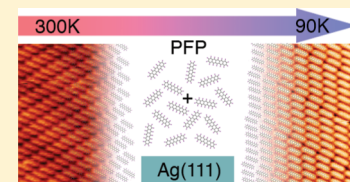
^{||}Dpto. de Física Aplicada I, Universidad del País Vasco, E-20018 Donostia-San Sebastián, Spain

[§]Department of Physics, University of California at Berkeley, Berkeley, California 94720, United States

Supporting Information

ABSTRACT: In-plane dislocation networks arise in both inorganic and organic films as a way of relieving the elastic strain that builds up at the substrate interface. In molecule/surface systems, supramolecular interactions are weak and more complex (compared to the atomic bonds in inorganic films), and their interplay with molecule–substrate interactions is very subtle, making it difficult to single out the driving force for a nanoscale dislocation pattern. On the basis of a combined experimental and theoretical work, we here show that periodic dislocations in a molecular PFP film are mainly driven by the optimization of molecule–substrate interactions. Compared to inorganic networks however, it implies a much lower energy imbalance, allowing a thermally induced transition from a low-energy strain dislocation pattern to a high-energy incommensurate moiré.

SECTION: Surfaces, Interfaces, Catalysis



Strain-relief networks and moiré patterns in monolayers are attractive because of their great potential as nanoscale growth templates for a variety of materials.^{1–5} Most examples of such nanoscale patterns involve inorganic materials.^{1–12} In organic layers, while moirés were already observed decades ago,^{13–16} only a few recent reports about strain-relief networks exist.^{17–21} In reality, textured organic substrates are better suited as templates due to their higher chemical stability.²² However, organic layer growth is inherently more complex than its inorganic analogue due to the additional internal degrees of freedom (orientational and vibrational) in molecules, as well as to the weakness of interactions (intermolecular and molecule–substrate).²³ As a result, the few examples of organic dislocation networks reported to date still lack a basic understanding of the underlying balance of interactions. In this work, we tackle this problem using the PFP/Ag(111) dislocation network^{18,19} as a model system. The combination of STM measurements with first-principle theoretical calculations allows us to quantitatively rationalize the hierarchy of interactions and hence to identify the mechanism responsible for the periodic dislocations. Hereby, we do not only put forward a new structural model for this important heterointerface but also provide seminal understanding of the role and subtleness of strain at metal–organic interfaces.

Strain is inherent to heterointerfaces; therefore, the important point in crystal growth is how the elastic stress is released. The scenario is apparently simple for a two-dimensional (2D) incommensurate monolayer, that is, one that crystallizes with its own lattice constant. Here, the strain may accommodate vertically, leading to a moiré-like undulation,

or laterally, giving rise to in-plane dislocation networks. Interestingly, some systems present both of these structures and can transition from one to the other.^{8,10,12,24,25} In such cases, the question that arises is which relaxation, vertical or lateral, dominates. Ag/Cu(111)¹² and Au/Ni(111)⁸ monolayers form moirés at low temperature (LT) that become triangular dislocation networks at room temperature (RT). The transition is irreversible, suggesting that the dislocation network is actually the lower-energy phase,⁸ hindered by the limited kinetics at LT. This hierarchy, lateral-over-vertical, is supported by experiments^{10,24} or model calculations²⁵ in which the atomic density, that is, the chemical potential, is significantly varied. On the basis of the present PFP/Ag(111) organic layer experiments and supported by our theoretical calculations, we demonstrate that for a nearly constant chemical potential, the dislocation network is the low-energy phase, which may transition to a higher-energy moiré structure by increasing the temperature.

Our LT STM measurements show that PFP monolayers on Ag(111) arrange into a highly crystalline structure with large faultless domains exceeding 100 nm (Figure 1). The molecules are in a flat-lying configuration with an oblique unit cell of dimensions $a = 8.8 \pm 0.9 \text{ \AA}$, $b = 17 \pm 1 \text{ \AA}$, and $\gamma = 62 \pm 2^\circ$. The long unit cell vector b is oriented along the close-packed direction of the substrate, though the long molecule axis very slightly deviates (approximately 3°) from this direction. Given

Received: January 12, 2012

Accepted: March 7, 2012

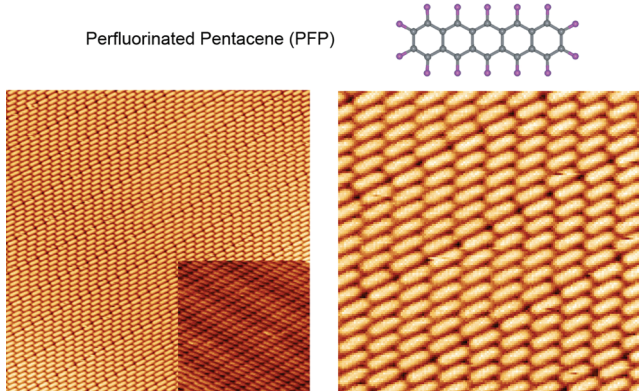


Figure 1. (Above) Chemical structure of the PFP molecule. (Bottom) (Left) $50 \text{ nm} \times 50 \text{ nm}$ image ($-1.37 \text{ V}, 9.08 \text{ pA}$) of PFP/Ag(111) showing the high crystallinity of the monolayer and periodic dislocations. (Right) $15 \text{ nm} \times 15 \text{ nm}$ image showing a close-up of the dislocation lines appearing every six molecule rows. PFP molecules appear as single peg-shaped features. (Inset) The moiré structure found at RT, which is free of lateral dislocations ($0.85 \text{ V}, 9.64 \text{ pA}$).

the hexagonal symmetry of the Ag(111) surface, six discrete domains are observed, these being three rotational domains and their corresponding mirror domains.

Additionally, a superstructure consisting of periodic dislocation lines in the direction of the long unit cell axis appears, usually every six molecules (Figure 1). Along these dislocation lines, the molecules end up side by side in a nearly rectangular cell, as opposed to laterally shifted like in their oblique unit cell (unit cells marked in red in Figure 2a). This side-by-side arrangement is expected to be energetically less favorable; the fluorine atoms are directly across from each other, enhancing electrostatic repulsion. This leads to an increased lateral distance between molecules (by $7 \pm 4\%$ as measured by STM, significantly lower than the 33% dilation associated with the recently proposed commensurate model^{18,19}) that lowers the packing density of the layer, thereby decreasing the energy gain associated with the molecule–substrate interactions.

Quantification of the molecule–substrate and intermolecular interactions, the balance of which leads to this specific arrangement, is obtained from density functional theory (DFT) calculations, all of which have been carried out through the GPAW code.²⁶ The study of layers of aromatic molecules deposited on a metallic surface through DFT calculations brings up the question, which exchange–correlation functional is most appropriate for the particular system in question. The performance of local density approximation (LDA),²⁷ general gradient approximation (GGA),²⁸ ab initio van der Waals (vdW-DFT),²⁹ and semiempirical van der Waals (DFT-D)³⁰ functionals for different systems has been extensively investigated in the literature. One of the main conclusions of these studies is that GGA functionals have a general tendency to underestimate adsorption energies and overestimate distances between the aromatic molecule and the metal.^{31–34} Another general trend is that LDA functionals yield shorter distances and stronger adsorption energies than DFT-D and vdW-DFT. However, it is not possible to know *a priori* which of them will give results closer to the experimental ones for a particular system, making it necessary to check this. From values reported in the literature, complemented with our own calculations, we conclude that LDA is the best choice to study this particular type of systems (see the Supporting Information)

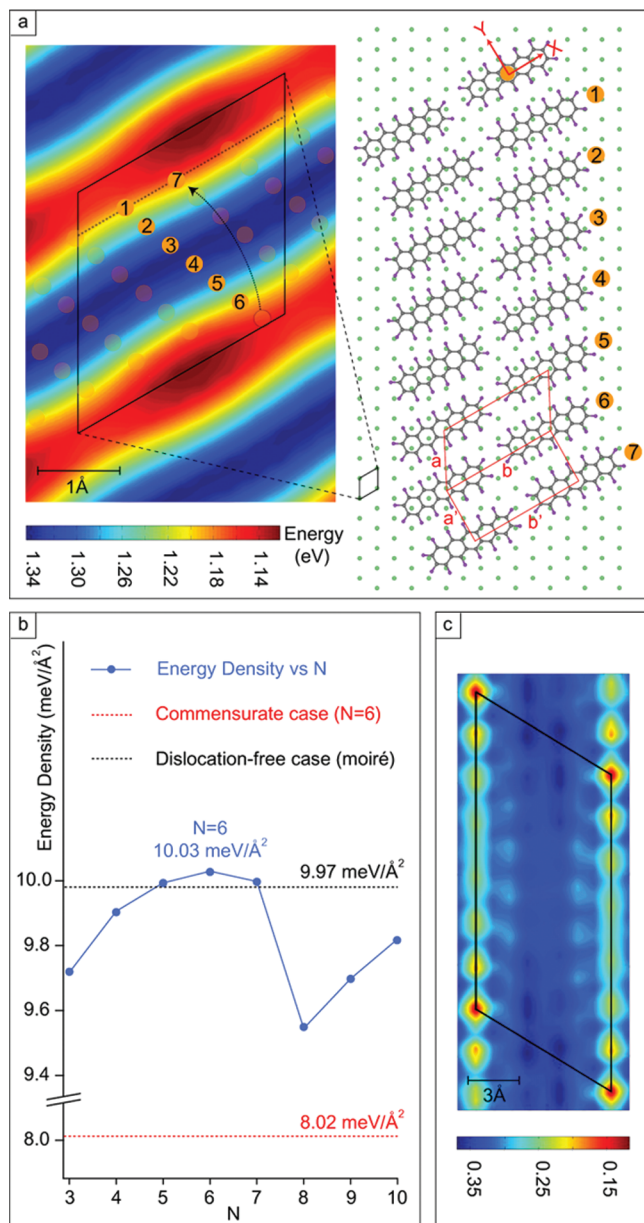


Figure 2. (a) Model for dislocations. The structure is commensurate in the direction of b but not in that of a. Oblique and rectangular cells are marked in red. Adsorption energy of the PFP molecule as a function of its position on the substrate. The numbers indicate the positions of molecules in the model structure, projected onto a single unit cell. It is essential for the model that the next group of molecules (7 and on) be aligned in the Y direction with the first group (1–6). (b) Energy densities for the system as a function of the dislocation periodicity (every N molecules along the a axis, blue), the dislocation-free case (black) and the commensurate case (red). (c) Adsorption energy for a molecule on an underlying PFP layer. The oblique unit cell of the underlying layer is marked, with the vertices corresponding to molecular centers.

and have therefore used it for the rest of the calculations in the present work.

The calculations can be divided in two parts. First, the molecule–substrate interactions were quantified; maintaining the molecular orientation observed in the experiment, the adsorption energy of a PFP molecule on the Ag(111) surface was calculated as a function of its displacement over the surface

(see Figure 2a). The calculations yielded a large adsorption energy ranging from 1.34 to 1.12 eV, depending on the molecule's adsorption site. As can be seen in the figure, there is a large variation in adsorption energy as the molecule is displaced in the Y direction, whereas the adsorption energy remains practically constant in the X direction. The reason for this lies in the size and shape of the molecule; its long axis, oriented in the X direction, is several times larger than the lattice spacing, making the displacement in this direction less perceptible. The calculations show that the adsorption of a molecule on the silver substrate is always favorable for the system. As a consequence, the more compact the arrangement of the layer, the higher the energy gain will be. A dislocation reduces the compactness by increasing the width of the unit cell by about 7%, thus effectively reducing the energy gain associated with the molecular adsorption by this amount, which is on the order of 0.08 eV.

In the second part of the calculations, we focus on the intermolecular interactions. We consider two contributions, intermolecular interactions neglecting the substrate and those mediated by it (see the Supporting Information for more details). Calculations yielded 0.06 and 0.03 eV, respectively, giving a total attractive intermolecular interaction energy of 0.09 eV for both the oblique and rectangular unit cells. Substrate-mediated interactions (SMI) are discussed in the literature,^{35,36} but to our knowledge, up until now, there have been few attempts to quantify them. Sykes et al. were able to experimentally determine the SMI of benzene on Au(111), finding it to be approximately 0.005 eV per molecule,³⁵ compared with a molecule–substrate interaction of 0.64 eV.³⁷ In view of these values, a SMI energy of 0.03 eV compared to a molecule–substrate interaction of around 1.2 eV as found in our PFP/Ag(111) system seems to be a reasonable result, considering the larger size and number of atoms in PFP compared to those for benzene.

The structural model obtained from our experiments is shown in Figure 2a. According to this model, the molecules arrange around the adsorption minimum (blue area) in their oblique configuration so as to maximize the energy gained from adsorption and optimize the packing density. As the molecules get farther from the equilibrium position (dark blue), the adsorption energy continuously decreases from molecule to molecule, until reaching a threshold value for which it becomes more favorable to form a dislocation, despite the loss of compactness, instead of maintaining the oblique configuration. (The situation should of course be symmetrical, as is shown in the figure; dislocations occur after molecule 6 and before molecule 1.) The molecules therefore shift to remain on a more favorable position on the substrate, adopting a rectangular cell.

We have performed theoretical calculations using the unit cell parameters obtained by STM in order to show that the formation of dislocations reduces the system's energy density. First, we consider a dislocation-free system. Given the incommensurability of the overlayer in the direction of a , molecules will occupy all positions on the substrate, that is, the molecule–substrate interaction energy per molecule will simply be the average value, 1.23 eV. The energy density in this case comes out to be 9.97 meV/ \AA^2 . Next, we consider the different possible dislocations that could occur as a function of their periodicity (after $N = 3$ –10 molecules along the a axis). As these are naturally a way to increase the energy gain of the system, we assume that the dislocation lines must minimize the overall system energy by keeping the molecules in a certain

range of adsorption energies. In order to do so, it is necessary for the dislocation to bring the next group of N molecules to a position equivalent to that of the first group, that is, there must be no displacement in the Y direction with respect to the previous group (alignment in Y). This guarantees that successive groups will remain in the region of minimum adsorption energy and not stray into less favorable areas. This is made clear in Figure 2a; the dotted line joining positions 1 and 7 marks the direction of constant Y . Taking the rectangular lattice angle as $\gamma = 90^\circ$ and the experimental oblique cell parameters,³⁸ we calculate the cell dilation necessary to keep the successive groups of molecules aligned in the Y direction for each N . All that is left now is to calculate the energy density in each case. The results are plotted in Figure 2b and show that for $4 < N < 8$, dislocations are an effective way to reduce the total energy of the system. The maximum energy gain is achieved for $N = 6$, the experimentally observed case, with an energy density of 10.03 meV/ \AA^2 . The difference with $N = 5$ and 7 is small, explaining why these are sometimes observed too.

By comparing the energy densities of the $N = 6$ case and the dislocation-free layer, we can obtain an estimate of the threshold energy associated with the formation of the dislocations. This difference is 0.06 meV/ \AA^2 . Such a small value is typically within DFT error margins. Therefore, while the energy variation with N is significant and unambiguously favors periodicities around $N = 6$, the reliability of the 0.06 meV/ \AA^2 difference with respect to the dislocation-free layer may be doubted. Interestingly, additional STM measurements at RT prove the correct order of magnitude of our DFT results and the subtlety of the energy balance responsible for such dislocation networks.

RT PFP/Ag(111) measurements show ordered layers with an oblique cell practically identical to that found at LT. However, instead of the dislocation lines, a voltage-independent modulation of contrast is observed along the same direction. This modulation is interpreted as a linear moiré pattern generated by the lattice mismatch between the overlayer and substrate (see Figure 1, inset), in which molecules on areas of same contrast are located on crystallographically equivalent substrate sites. This occurs with a longer periodicity as compared to the dislocations, after around eight molecules in the direction of the short axis. An explanation for the differences between LT and RT monolayers may be that the strain associated with the mismatch in PFP–substrate positions responsible for the dislocations at LT is compensated at RT by substrate phonons and molecular vibrations. Multiplying the area of the unit cell times 0.06 meV/ \AA^2 yields about 8 meV per molecule,³⁹ which is of the order of the thermal energy at LT ($kT \approx 8$ meV) and far below that of RT ($kT \approx 26$ meV), as would be expected from the presence of the dislocations at LT and their disappearance at RT.

Note that this model is essentially different from that proposed in previous work,^{18,19} where the structure is proposed to be commensurate throughout the layer. We discard a commensurate structure because it fails to explain the periodic dislocation lines; upon commensuration, all molecules are energetically alike; intermolecular interaction energy is indeed accumulated throughout the layer at the expense of an optimized molecule–substrate matching, but that energy is always the same. Thus, if the oblique arrangement is energetically favorable for one molecule, it should be the same for all of the next ones, and a dislocation would not be favored at any time. We performed calculations for the

commensurate case and found the intermolecular interactions of the commensurate oblique cell to be strongly repulsive (-0.29 eV per molecule) due to the proximity of the fluorine atoms of neighboring molecules. Considering each molecule to be on the most favorable adsorption site (1.34 eV), the energy density of the commensurate layer comes out to be 8.02 meV/ \AA^2 , well below the 10.03 meV/ \AA^2 of the noncommensurate structure that we propose. (See Figure 2b for a comparison of all calculated energy densities.)

We also discard a bistability of relatively similar energy configurations (oblique versus rectangular unit cells) as the source for the dislocation formation. This was proposed, for example, for the linear dislocation patterns at the TCNQ/Cu(100) interface.²¹ However, that should lead to a random distribution of the dislocation lines. Instead, the well-defined periodicity that we observe suggests there is an additional elastic stress contribution that leads to periodic accumulation and release of stress throughout the layer, as suggested above.

Measurements of the second-layer growth at LT are summarized in Figure 3 for two different coverages. Upon

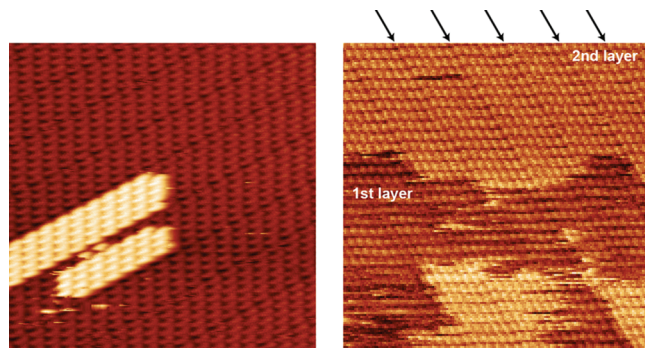


Figure 3. $30 \text{ nm} \times 30 \text{ nm}$ images ($-1.3 \text{ V}, 9 \text{ pA}$) of initial (a) and more advanced (b) stages of second-layer growth. In (b), it becomes clear that the dislocation pattern is transferred to the second layer. Arrows mark second-layer dislocation lines.

increasing coverage, it becomes clear that the dislocation lines arising from the interactions at the molecule–substrate interface are transferred to the second layer (Figure 3b), contrasting with previous reports.^{18,19} While this might be ascribed to the different preparation conditions, DFT calculations support the convenience of dislocation transfer to the second layer. The adsorption energy of a PFP molecule azimuthally oriented as those in the first monolayer has been calculated by DFT as a function of its lateral displacement (Figure 2d). The maximum adsorption energy (0.35 eV) is significantly lower than that of PFP on Ag(111) and explains, in combination with a low Ehrlich–Schwoebel barrier, the absence of second-layer islands until the first layer is complete. As in the case of PFP on the silver surface, there is a strong variation in the direction of a and only a minor modulation along b . However, given that at the dislocation lines, the molecules are not only shifted along b but are also subject to an increased distance along a , the dislocations are transferred to the second layer to avoid an accumulated mismatch along a and its associated energy loss. With these results depending only on molecule–molecule interactions, they can be extrapolated to subsequent layers. However, the calculations assume planarity of the overlayer molecules and are therefore not applicable as the molecules deviate from a planar arrangement. Transfer of the dislocation pattern to subsequent layers is therefore

expected to take place until new tilted molecular configurations set in in upper layers (according to Goetzen et al., from the third layer onward).¹⁸

To summarize, by combining our STM results with theoretical calculations of intermolecular, substrate-mediated, and molecule–substrate interactions, we have been able to put forward a model that successfully explains the existence of a dislocation network at the PFP/Ag(111) interface at LT that is replaced by a moiré pattern at RT. Key to this thermal dependence are the low energies involved in the strain relief as compared to similar systems at inorganic heterointerfaces. We thereby take one further step toward understanding the role and interplay of all of the different interactions that drive the formation of molecular overlayers at metal–organic interfaces.

EXPERIMENTAL SECTION

The Ag(111) sample was prepared by cycles of Ar sputtering at 800 eV at an Ar partial pressure of 2.6×10^{-6} mbar followed by annealing to 300 – 400 °C. Deposition of PFP took place at RT from a homemade Knudsen cell and was monitored with a quartz crystal microbalance. The sample was subsequently cooled with LN₂ to around 90 K and measured with a VT-Omicron STM (base pressure $< 3 \times 10^{-10}$ mbar). Constant current mode was used, with electrochemically etched W tips. Our PFP/Ag(111) samples were prepared by accurate monolayer coverage deposition at RT and no postannealing treatments, instead of the multilayer desorption method used in previous reports.^{18,19}

ASSOCIATED CONTENT

Supporting Information

Further details regarding the theoretical DFT calculations, including energy definitions, comparison of functional performances, and image charge model for PFP/Ag(111) interaction. Experimental support for the molecular orientation determination. This material is available free of charge via the Internet at <http://pubs.acs.org>.

AUTHOR INFORMATION

Corresponding Author

*E-mail: dgotezya@berkeley.edu.

Notes

The authors declare no competing financial interest.

ACKNOWLEDGMENTS

This work was supported by the Spanish MICINN (MAT2010-21156-C03-01 and -C03-03) and the Basque Government (IT-257-07).

ADDITIONAL NOTE

During the review process, we became aware of a new work published about the PFP/Ag(111) interface as a function of temperature.⁴⁰ A structural phase transition is observed starting at 130 K, in line with our results. However, the transition is claimed to occur between a commensurate and a disordered PFP overlayer structure. In this Letter, we prove the noncommensurate nature of the LT phase and unambiguously show an ordered PFP monolayer at RT. Differences in the preparation method could play a role in some of the discrepancies.

REFERENCES

- (1) Chambliss, D. D.; Wilson, R. J.; Chiang, S. Nucleation of Ordered Ni Island Arrays on Au(111) by Surface-Lattice Dislocations. *Phys. Rev. Lett.* **1991**, *66*, 1721–1724.
- (2) Brune, H.; Giovannini, M.; Bromann, K.; Kern, K. Self-Organized Growth of Nanostructure Arrays on Strain-Relief Patterns. *Nature* **1998**, *394*, 451–453.
- (3) Pohl, K.; Bartelt, M. C.; de la Figuera, J.; Bartelt, N. C.; Hrbek, J.; Hwang, R. Q. Identifying the Forces Responsible for Self-Organization of Nanostructures at Crystal Surfaces. *Nature* **1999**, *397*, 238–241.
- (4) Ait-Mansour, K.; Treier, M.; Ruffieux, P.; Bieri, M.; Jaafar, R.; Görning, P.; Fasel, R.; Gröning, O. Template-Directed Molecular Nanostructures on the Ag/Pt(111) Dislocation Network. *J. Phys. Chem. C* **2009**, *113*, 8407–8411.
- (5) Fernández, L.; Corso, M.; Schiller, F.; Ilyn, M.; Holder, M.; Ortega, J. E. Self-Organized Growth of High Density Magnetic Co Nanodot Arrays on a Moiré Template. *Appl. Phys. Lett.* **2010**, *96*, 013107.
- (6) Böhringer, M.; Jiang, Q.; Berndt, R.; Schneider, W.-D.; Zegenhagen, J. Discommensurations, Epitaxial Growth and Island Formation in Ge(111):Cu. *Surf. Sci.* **1996**, *367*, 245–260.
- (7) Shiryaev, S.; Jensen, F.; Hansen, J.; Petersen, J.; Larsen, A. Nanoscale Structuring by Misfit Dislocations in $\text{Si}_{1-x}\text{Ge}_x/\text{Si}$: Epitaxial Systems. *Phys. Rev. Lett.* **1997**, *78*, 503–506.
- (8) Jacobsen, J.; Pleth Nielsen, L.; Besenbacher, F.; Stensgaard, I.; Lægsgaard, E.; Rasmussen, T.; Jacobsen, K. W.; Nørskov, J. K. Atomic-Scale Determination of Misfit Dislocation Loops at Metal–Metal Interfaces. *Phys. Rev. Lett.* **1995**, *75*, 489–492.
- (9) Hwang, R. Q.; Hamilton, J. C.; Stevens, J. L.; Foiles, S. M. Near-Surface Buckling in Strained Metal Overlayer Systems. *Phys. Rev. Lett.* **1995**, *75*, 4242–4245.
- (10) Corso, M.; Fernández, L.; Schiller, F.; Ortega, J. E. Au(111)-Based Nanotemplates by Gd Alloying. *ACS Nano* **2010**, *4*, 1603–1611.
- (11) Howe, J. D.; Bhopale, P.; Tiwary, Y.; Fichthorn, K. Patterns in Strained-Layer Heteroepitaxy: Beyond the Frenkel–Kontorova Model. *Phys. Rev. B* **2010**, *81*, 121410.
- (12) Bendounan, A.; Cercellier, H.; Fagot-Revrat, Y.; Kierren, B.; Yurov, V. Y.; Malterre, D. Modification of Shockley States Induced by Surface Reconstruction in Epitaxial Ag Films on Cu(111). *Phys. Rev. B* **2003**, *67*, 165412.
- (13) Rabe, J. P.; Buchholz, S. Commensurability and Mobility in 2-Dimensional Molecular-Patterns on Graphite. *Science* **1991**, *253*, 424–427.
- (14) Strohmaier, R.; Ludwig, C.; Petersen, J.; Gompf, B.; Eisenmenger, W. STM Investigations of C_6Br_6 on HOPG and MOS_2 . *Surf. Sci.* **1994**, *318*, L1181.
- (15) Ahlund, J.; Schnadt, J.; Nilson, K.; Gothelid, E.; Schiessling, J.; Besenbacher, F.; Martensson, N.; Puglia, C. The Adsorption of Iron Phthalocyanine on Graphite: A Scanning Tunnelling Microscopy Study. *Surf. Sci.* **2007**, *601*, 3661–3667.
- (16) Ilan, B.; Florio, G. M.; Hybertsen, M. S.; Berne, B. J.; Flynn, G. W. Scanning Tunneling Microscopy Images of Alkane Derivatives on Graphite: Role of Electronic Effects. *Nano Lett.* **2008**, *8*, 3160–3165.
- (17) Wei, Y.; Robey, S. W.; Reutt-Robey, J. E. TiOPc Molecular Dislocation Networks as Nanotemplates for C_{60} Cluster Arrays. *J. Am. Chem. Soc.* **2009**, *131*, 12026–12027.
- (18) Götz, J.; Schwalb, C. H.; Schmidt, C.; Mette, G.; Marks, M.; Höfer, U.; Witte, G. Structural Evolution of Perfluoro-Pentacene Films on Ag(111): Transition from 2D to 3D Growth. *Langmuir* **2011**, *27*, 993–999.
- (19) Wong, S. L.; Huang, H.; Huang, Y. L.; Wang, Y. Z.; Gao, X. Y.; Suzuki, T.; Chen, W.; Wee, A. T. S. Effect of Fluorination on the Molecular Packing of Perfluoropentacene and Pentacene Ultrathin Films on Ag(111). *J. Phys. Chem. C* **2010**, *114*, 9356–9361.
- (20) Oison, V.; Koudia, M.; Abel, M.; Porte, L. Influence of Stress on Hydrogen-Bond Formation in a Halogenated Phthalocyanine Network. *Phys. Rev. B* **2007**, *75*, 035428.
- (21) Tseng, T.-C.; Urban, C.; Wang, Y.; Otero, R.; Tait, S. L.; Alcamí, M.; Ecija, D.; Trelka, M.; Gallego, J. M.; Lin, N.; et al. Charge Transfer-Induced Structural Rearrangements at Both Sides of Organic/Metal Interfaces. *Nat. Chem.* **2010**, *2*, 374–379.
- (22) Park, S.; Lee, D. H.; Xu, J.; Kim, B.; Hong, S. W.; Jeong, U.; Xu, T.; Russell, T. P. Macroscopic 10-Terabit-per-Square-Inch Arrays from Block Copolymers with Lateral Order. *Science* **2009**, *323*, 1030–1033.
- (23) Schreiber, F. Organic Molecular Beam Deposition: Growth Studies beyond the First Monolayer. *Phys. Status Solidi A* **2004**, *201*, 1037–1054.
- (24) Bott, M.; Hohage, M.; Michely, T.; Comsa, G. Pt(111) Reconstruction Induced by Enhanced Pt Gas-Phase Chemical-Potential. *Phys. Rev. Lett.* **1993**, *70*, 1489–1492.
- (25) Pushpa, R.; Narasimhan, S. Reconstruction of Pt(111) and Domain Patterns on Close-Packed Metal Surfaces. *Phys. Rev. B* **2003**, *67*, 205418.
- (26) Enkovaara, J.; Rostgaard, C.; Mortensen, J. J.; Chen, J.; Dulak, M.; Ferrighi, L.; Gavnholt, J.; Glinsvad, C.; Haikola, V.; Hansen, H. A.; et al. Electronic Structure Calculations with GPAW: A Real-Space Implementation of the Projector Augmented-Wave Method. *J. Phys.: Condens. Matter* **2010**, *22*, 253202.
- (27) Perdew, J. P.; Zunger, A. Self-Interaction Correction to Density-Functional Approximations for Many-Electron Systems. *Phys. Rev. B* **1981**, *23*, 5048.
- (28) Perdew, J. P.; Burke, K.; Ernzerhof, M. Generalized Gradient Approximation Made Simple. *Phys. Rev. Lett.* **1996**, *77*, 3865–3868.
- (29) Dion, M.; Rydberg, H.; Schroder, E.; Langreth, D. C.; Lundqvist, B. I. Van der Waals Density Functional for General Geometries. *Phys. Rev. Lett.* **2004**, *92*, 246401.
- (30) Grimme, S. Semiempirical GGA-Type Density Functional Constructed with a Long-Range Dispersion Correction. *J. Comput. Chem.* **2006**, *27*, 1787–1799.
- (31) Toyoda, K.; Hamada, I.; Lee, K.; Yanagisawa, S.; Morikawa, Y. Density Functional Theoretical Study of Pentacene/Noble Metal Interfaces with van der Waals corrections: Vacuum Level Shifts and Electronic Structures. *J. Chem. Phys.* **2010**, *132*, 134703.
- (32) Toyoda, K.; Hamada, I.; Lee, K.; Yanagisawa, S.; Morikawa, Y. Density Functional Theoretical Study of Perfluoropentacene/Noble Metal Interfaces with van der Waals Corrections: Adsorption States and Vacuum Level Shifts. *J. Phys. Chem. C* **2011**, *115*, 5767–5772.
- (33) Vanin, M.; Mortensen, J. J.; Kelkkanen, A.; García-Lastra, J. M.; Thygesen, K. S.; Jacobsen, K. W. Graphene on Metals: A van der Waals Density Functional Study. *Phys. Rev. B* **2010**, *81*, 081408.
- (34) Wellendorff, J.; Kelkkanen, A.; Mortensen, J.; Lundqvist, B.; Bligaard, T. RPBE-vdW Description of Benzene Adsorption on Au(111). *Top. Catal.* **2010**, *53*, 378–383.
- (35) Sykes, E. C. H.; Mantooh, B. A.; Han, P.; Donhauser, Z. J.; Weiss, P. S. Substrate-Mediated Intermolecular Interactions: A Quantitative Single Molecule Analysis. *J. Am. Chem. Soc.* **2005**, *127*, 7255–7260.
- (36) Sykes, E. C. H.; Han, P.; Kandel, S. A.; Kelly, K. F.; McCarty, G. S.; Weiss, P. S. Substrate-Mediated Interactions and Intermolecular Forces between Molecules Adsorbed on Surfaces. *Acc. Chem. Res.* **2003**, *36*, 945–953.
- (37) Syomin, D.; Kim, J.; Koel, B. E.; Ellison, G. B. Identification of Adsorbed Phenyl (C_6H_5) Groups on Metal Surfaces: Electron-Induced Dissociation of Benzene on Au(111). *J. Phys. Chem. B* **2001**, *105*, 8387–8394.
- (38) Parameter a was fixed to $a = 8.87\text{\AA}$ in agreement with the 7% dilation of the rectangular unit cell resulting from the model with $N = 6$.
- (39) The exact value should be taken with care not only because of DFT error margins but also because differences in the thermal expansion coefficients between the organic layer and the Ag substrate may additionally modify the interaction potential landscape.
- (40) Marks, M.; Schmidt, C.; Schwalb, C. H.; Breuer, T.; Witte, G.; Hofer, U. Temperature-Dependent Structural Phase Transition at the Perfluoropentacene/Ag(111) Interface. *J. Phys. Chem. C* **2012**, *116*, 1904–1911.

Supporting information for:

Understanding periodic dislocations in 2D supramolecular crystals: the PFP/Ag(111) interface

E. Goiri¹, J. M. García-Lastra², M. Corso¹, Z. M. Abd El-Fattah³, J. E. Ortega^{1,3,4}, and D. G. de Oteyza^{3,5}

¹*Donostia International Physics Center, Paseo Manuel Lardizabal 4, E-20018 Donostia-San Sebastián, Spain*

²*Technical University of Denmark, Dept. of Physics, DK-2800 Copenhagen, Denmark*

³*Centro de Física de Materiales CSIC/UPV-EHU-Materials Physics Center, E-20018 Donostia-San Sebastián, Spain,*

⁴*Universidad del País Vasco, Dpto. de Física Aplicada I, E-20018 Donostia-San Sebastián, Spain*

⁵*University of California at Berkeley, Department of Physics, Berkeley, CA 94720, USA*

*E-mail: dgotezya@berkeley.edu

Contents

- 1. Energy Definitions**
- 2. Functionals performance for Pentacene and PFP on Ag(111)**
- 3. Image charge model of PFP-Ag(111) interaction**
- 4. Experimental determination of the azimuthal molecular orientation**
- 5. References**

1. Energy definitions

For the DFT calculations it was crucial to separate the energy contributions in two terms:

i. The PFP-Ag interaction, $E_{PFP\text{-}Ag}$, defined as

$$E_{PFP\text{-}Ag} = E(PFP@Ag) - E(Ag) - E(PFP);$$

where $E(PFP@Ag)$, $E(Ag)$, and $E(PFP)$ are total energies of an adsorbed system, a clean Ag(111) surface, and an isolated PFP molecule, respectively.

ii. The PFP-PFP nearest neighbor interaction, $E_{PFP\text{-}PFP}$, defined as

$$E_{PFP\text{-}PFP} = [E(PFP_1+PFP_2@Ag) - E(Ag) - 2 \cdot E(PFP)] - [E(PFP_1@Ag) - E(Ag) - E(PFP)] - [E(PFP_2@Ag) - E(Ag) - E(PFP)] = E(PFP_1+PFP_2@Ag) + E(Ag) - E(PFP_1@Ag) - E(PFP_2@Ag);$$

where $E(PFP_1+PFP_2@Ag)$ and $E(PFP_i@Ag)$; ($i = 1; 2$) are the total energies of an adsorbed system with two molecules placed at sites 1 and 2, and an adsorbed system with one molecule place at site i , respectively.

In order to analyze these terms we carried out DFT calculations by means of the GPAW code¹, using periodic boundary conditions and the Local Density Approximation (LDA). $E_{PFP\text{-}Ag}$ (Fig. 2c of the manuscript) was mapped using the relative position of the PFP molecule center with respect to the origin of the Ag(111) surface unit cell as the coordinate. To model the metal-molecule interface we used a super-cell containing three layers of Ag(111) with 7×8 atoms in each layer ($20.22 \times 23.11 \text{ \AA}$). This size ensures that the interaction between PFP replicas is negligible. The Ag(111) slab and PFP molecule structures were kept fixed. Thus the only degree of freedom was the displacement of PFP molecule over the Ag(111) surface. $E_{PFP\text{-}PFP}$ was evaluated using the same super-cell, but placing two PFP molecules instead of one. The two PFP molecules were arranged in the two different configurations shown in Fig. 2a of the manuscript. Again the size of the super-cell guarantees that the interaction between a PFP pair and its replicas is insignificant. The PFP-PFP nearest neighbor interaction was also calculated in vacuo, without the presence of the Ag(111) substrate, using the same calculation parameters. $E_{PFP\text{-}PFP}$ in vacuo is simply defined as

$$E_{PFP\text{-}PFP} = E(PFP_1+PFP_2) - 2 \cdot E(PFP)$$

For both types of calculations, PFP molecules lie flat at $Z = 3.14 \text{ \AA}$ above the surface followed by 12 \AA of vacuum. We previously determined the distance $Z = 3.14 \text{ \AA}$, which is very close to the experimental one $Z = 3.16 \text{ \AA}$ measured by Duhm et al.^{2, S2} by means of a geometry optimization. The energy of formation of

the bilayer with respect to the lateral displacement of the layers (Fig. 2d of the manuscript) was also mapped similarly to the E_{PFP-Ag} mapping. In this case we only consider two parallel PFP layers in the model, without including the Ag(111) substrate. The interlayer distance, $D = 3.46\text{\AA}$, was previously determined through a geometry optimization and kept fixed during the mapping.

2. Functionals performance for PFP on Ag(111) and Pentacene on Au(111).

In the case of PFP on Ag(111) the calculated Ag-PFP distances can be compared with the experimental one ($Z = 3.16 \text{ \AA}$) measured recently by Duhm et al.² Unfortunately, there is no experimental data for the PFP/Ag(111) adsorption energy. However, it is possible to compare the calculated and experimental adsorption energies for a similar system to PFP/Ag(111), such as Pentacene (PEN) on Au(111). Toyoda et al. have studied the performance of GGA, DFT-D and vdW-DFT functional for these two systems. In the present work we have completed the study, including the LDA results (see Table 1). Regarding the distance in the PFP/Ag(111) system, the closest result to the experimental one is given by LDA. DFT-D shows a very good performance as well. By contrast, vdW-DFT and PBE overestimate significantly the experimental figure. Concerning the energetics in the PEN/Au(111) system, it is again LDA which renders the value closest to the experimental one. Whereas the vdW-DFT value is also in very good agreement, DFT-D gives the worst result. These results justify our LDA choice for the calculations in the present work.

Table 1. Calculated equilibrium distances (Z) and adsorption energies (E_{ads}) for PFP/Ag(111) and PEN/Au(111) using LDA, GGA, vdW-DFT and DFT-D functionals. The experimental distance for PFP/Ag(111) and the experimental adsorption energy for PEN/Au(111) are also shown.

	LDA (PZ)		GGA (PBE)		vdW-DFT		DFT-D		Experimental	
	$Z(\text{\AA})$	$E_{\text{ads}}(\text{eV})$	$Z(\text{\AA})$	$E_{\text{ads}}(\text{eV})$	$Z(\text{\AA})$	$E_{\text{ads}}(\text{eV})$	$Z(\text{\AA})$	$E_{\text{ads}}(\text{eV})$	$Z(\text{\AA})$	$E_{\text{ads}}(\text{eV})$
PEN/Au(111)	3.0 ^e	1.55 ^e	3.7 ^a	0.14 ^a	3.7 ^a	1.66 ^a	3.2 ^a	2.51 ^a	---	1.1 ^b
PFP/Ag(111)	3.14 ^e	1.34 ^e	4.2 ^c	0.12 ^c	3.7 ^c	1.71 ^c	3.2 ^c	2.40 ^c	3.16 ^d	---

^a Ref.3, ^b Ref.4, ^c Ref.5, ^d Ref.2, ^e Present work.

3. Image charge model of PFP-Ag(111) interaction

It has been measured that pentacene molecules on Au(111) do not lie flat parallel to the metal surface, but they are tilted⁷. The cause of this tilting is that pentacene-pentacene interaction is enhanced through it⁸. However, such a tilting has not been reported for PFP on Ag(111)². Why is that? One of the main differences between PFP and pentacene is that C-F bonds in PFP are strongly polar while C-H bonds in pentacene are not. The C-F dipoles in PFP are attracted by metallic surfaces through an image charge potential. Figure S1 shows how this attraction decays if the molecule is tilted along its long axis (the same happens if the molecule is tilted along its short axis). In the model we have considered the PFP atoms as point charges under a classical image charge potential ($V = -Z/4$, where Z is the height of the molecule above the metal surface). We have used the calculated Bader charges⁹ (fluorine are negative charged and the carbons of the edges are positively charged, whereas the inner carbons are neutral). The molecule is tilted along its long axis imposing the condition that the closest atom of the PFP to the Ag(111) surface remains at $Z=3.14$ Å. The model shows that most of the binding energy between PFP and the Ag(111) surface comes from the image charge potential (0.8 eV). It also shows that the image charge potential is a driving force to keep polar molecules parallel metallic surfaces.

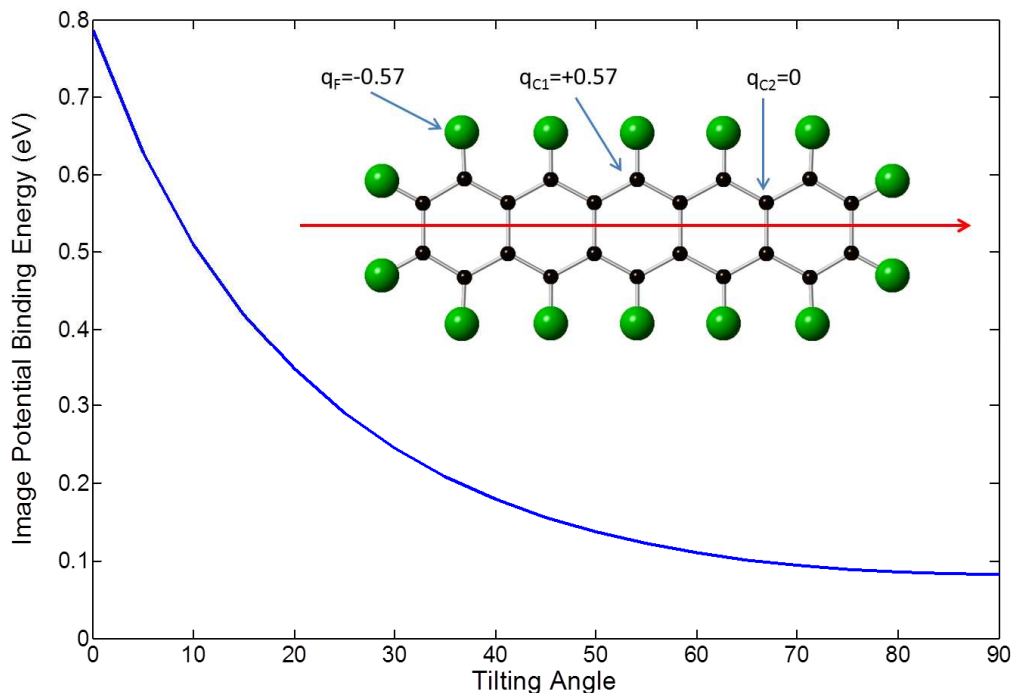


Figure S1. Image potential binding energy of PFP in Ag(111) vs. the tilting angle along the long axis of the molecule (red arrow in the inset figure) for a fixed PFP-Ag distance $Z=3.14$ Å. Positive energies mean attractive interaction.

4. Experimental determination of the azimuthal molecular orientation

Well-defined steps are known to follow preferentially the compact high-symmetry directions of the crystal. Figure S2 shows an STM image of the PFP layer on a Ag(111) region with well-defined parallel steps along the [1-10] direction. The dislocation lines precisely follow the direction of these steps.

Alternatively, due to the C₆ symmetry of the underlying silver surface, in combination with the oblique unit cell of the PFP overlayer, six distinct domains are observed: three rotational domains plus their corresponding twin domains, to which they are related by reflection through a plane along a high-symmetry direction. Analysis of the orientations of twin domains allows the determination of the substrate high-symmetry directions. Comparison of such direction with that of the dislocation lines corroborates their parallel alignment.

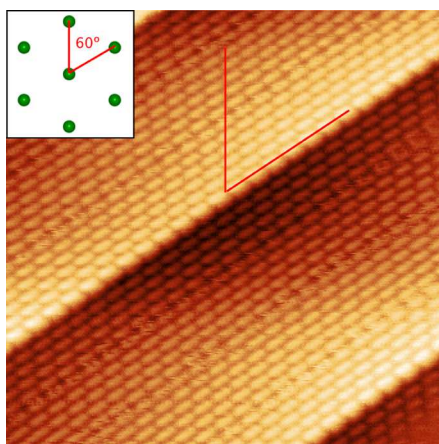


Figure S2. STM image of PFP/Ag(111) in a region of well-defined parallel substrate steps known to follow the [1-10] direction. The inset represents the hexagonal arrangement of the Ag surface atoms, with the [1-10] and [0-11] directions marked in red. The same directions are over imposed on the STM image.

5. References

1. J. Enkovaara, C. Rostgaard, J. J. Mortensen, J. Chen, M. Dulak, L. Ferrighi, J. Gavnholt, C. Glinsvad, V. Haikola, H. A. Hansen, H. H. Kristoffersen, M. Kuisma, A. H. Larsen, L. Lehtovaara, M. Ljungberg, O. Lopez-Acevedo, P. G. Moses, J. Ojanen, T. Olsen, V. Petzold, N. A. Romero, J. Stausholm-Moller, M. Strange, G. A. Tritsaris, M. Vanin, M. Walter, B. Hammer, H. Hakkinen, G. K. H. Madsen, R. M. Nieminen, J. K. Norskov, M. Puska, T. T. Rantala, J. Schiotz, K. S. Thygesen and K. W. Jacobsen, *Journal of Physics-Condensed Matter* **22** (25), 253202 (2010).
2. S. Duhm, S. Hosoumi, I. Salzmann, A. Gerlach, M. Oehzelt, B. Wedl, T. L. Lee, F. Schreiber, N. Koch, N. Ueno and S. Kera, *Physical Review B* **81** (4), 045418 (2010).
3. K. Toyoda, I. Hamada, K. Lee, S. Yanagisawa and Y. Morikawa, *Journal of Chemical Physics* **132** (13), 134703 (2010).
4. C. B. France, P. G. Schroeder, J. C. Forsythe, B. A. Parkinson, *Langmuir* **19**, 1274–1281 (2003).
5. K. Toyoda, I. Hamada, K. Lee, S. Yanagisawa and Y. Morikawa, *Journal of Physical Chemistry C* **115** (13), 5767-5772 (2011).
6. E. Mete, I. Demiroglu, M. F. Danisman and S. Ellalioglu, *Journal of Physical Chemistry C* **114** (6), 2724-2729 (2010).
7. D. Kaefer, L. Ruppel and G. Witte, *Physical Review B* **75** (8), 085309 (2007).
8. H. Li, Y. Duan, V. Coropceanu and J.-L. Bredas, *Organic Electronics* **10** (8), 1571-1578 (2009).
9. R. F. W. Bader, *Chemical Reviews* **91** (5), 893-928 (1991).